Granular Matter manuscript No.
(will be inserted by the editor)

Sticking of adhesive particles in elasto-plastic collisions

A. Singh, V. Magnanimo and S. Luding
Multi Scale Mechanics, CTW,
MESA+, UTwente,
P.O.Box 217, 7500 AE Enschede,
Netherlands,
e-mail: a.singh@ctw.utwente.nl

Abstract The pairwise interaction between dry, elasto-plastic, adhesive particles is the subject of this study – where particles are different from the well understood case of perfect, homogeneous spheres. We propose a simplified (piece-wise linear) model that combines a short-ranged (van der Waals type) attractive force with an advanced, flexible, normal contact force law. This mesoscopic model is applicable in dynamic, collisional as well as quasi-static, dense and confined situations.
Using simple energy considerations, an analytical solution for the coefficient of restitution e_n is derived, as function of the initial relative velocity – and validated by the numerical solutions of pairwise collisions. The relative influence of different sources of dissipation induces two sticking regimes, one at very low and one at high impact velocities. Very energetic collisions could avoid the sticking, either due to the elastic particle-core in the model, or due the change of phenomenology, e.g. due to fragmentation (not discussed, since this regime is beyond the reach of the model). The limits of the sticking regimes and the finite contact-overlaps, which sticking particles end up with, are reported and the influence of additional viscous dissipation on the pair collision dynamics is discussed.
Keywords: Particle Contact Models, Adhesion, Elasto-Plastic Material, Core-Shell materials, Energy dissipation

Nomenclature

m_i	:	mass of i^{th} particle.
a_i	:	Radius of i^{th} particle.
m_r	:	Reduced mass of two particles.
δ	:	Contact overlap between particles.
k	:	Spring stiffness.
v_i	:	Relative velocity before collision.
v_f	:	Relative velocity after collision.
v^n	:	Normal component of relative velocity.
e_n	:	Coefficient of restitution.
k_1	:	Slope of loading plastic branch.
k_2	:	Slope of unloading and reloading elastic branch.
k_p	:	Slope of unloading and reloading limit elastic branch.
k_c	:	Slope of irreversible, tensile adhesive branch.
v_p	:	Relative velocity before collision for which the limit case of overlap is reached.
$\delta_{\max}$	:	Maximum overlap between particles for a collision.
$\delta^p_{\max}$	:	Maximum overlap between particles for the limit case.
δ_0	:	Force free overlap $\cong$ plastic contact deformation.
$\delta_{\min}$	:	Overlap between particles at the maximum negative attractive force.
δ_c	:	Kinetic Energy free overlap between particles.

1 Introduction

Flows of granular materials are ubiquitous in industry and nature. For this reason, the past decade has witnessed a strong interest in better understanding granular materials. Especially, the impact of fine particles with particles/surfaces is a fundamental problem. The interaction force between two particles is a combination of elasto-plastic deformation, viscous dissipation, and adhesion – both due to contact and long-range forces.

Different regimes are observed for two colliding particles: For example a particle can either stick to another particle/surface or it rebounds, depending upon the relative strength of adhesion and impact velocity, size and material parameters. This problem needs to be studied in detail, as it forms the base for understanding more complex, many-particle flows in realistic systems, related to e.g. astrophysics (dust agglomeration, Saturn's rings) or industrial processes (handling of fine powders, filling and discharging of silos).

Particularly interesting is the interaction mechanism for adhesive materials like, e.g. asphalt, ice particles or clusters/agglomerates of fine powders, that can be physically visualized as having an outer shell with a rather stiff, elastic inner core. Due to the inhomogeneity of such materials, their non-sphericity, and their surface irregularity, it can not be the goal to include all details into a contact model – as presented here – but rather one has to catch the essential phenomena and ingredients, finding a compromise between simplicity and realistic contact mechanics.

Computer simulations have turned out to be a powerful tool to investigate the physics of particulate systems, especially valuable as there is no generally accepted theory of granular flows so far, and experimental difficulties are considerable. A very popular simulation scheme is an adaptation of the classical Molecular Dynamics technique called Discrete Element Method (DEM) (for details see Refs. [2, 4, 9, 14, 17, 18, 29, 33, 37]). It consists of integrating Newton's equations of motion for a system of "soft", deformable grains, starting from a given initial configuration. DEM has been successfully applied to adhesive particles, if a proper force-overlap model (contact model) is given.

Brilliantov et al. [3] investigated the collision of adhesive viscoelastic spheres and presented a general analytical expression for their collision dynamics, but we rather turn to plastic contact deformations in the following. The JKR model [12] is a widely accepted adhesion model for elastic spheres and gives an expression for the normal force. Later Derjaguin et al. [7] considered that the attractive forces act only just inside and outside the contact zone, where surface separation is small. One interesting model for dry adhesive particles was proposed by Molerus [23, 24], that explained consolidation and non-rapid flow of adhesive particles in terms of adhesion forces at particle contact. Thornton and Yin [32] compared the results of elastic spheres with and without adhesion and Thornton, later on in Ref. [31], extended this work to adhesive elasto-plastic spheres. Molerus's model was further developed by Tomas et al., who introduced a contact model [34–36] that couples elasto-plastic contact behavior with non-linear adhesion and hysteresis, which involves dissipation and a history (compression) dependent adhesive force. The contact model subsequently proposed by Luding [18, 21, 22] works in the same spirit as the one of Tomas [35], only reducing complexity by using piece-wise linear branches in an otherwise still highly non-linear contact model. Note that in the reference work [18], the short ranged force beyond contact was not specified as in the present study. Complex details like a possible non-linear Hertzian law, for small deformation, and non-linear load-unload hysteresis are over-simplified in the model. This is partly due to the lack of experimental reference data or theories, but also to keep the model as simple as possible. The model contains the basic mechanisms, elasticity, plasticity and adhesion as relevant for fine, dry powders and shell-core materials. A possible connection between the microscopic contact model and the macroscopic, continuum description for adhesive particles was recently proposed by Luding and Alonso-Marroquin [19].

When two particles collide, the behavior is intermediate between the extremes of perfectly elastic and fully inelastic, possibly fragmenting collisions. The elasticity of the collision can be best described by the coefficient of restitution, which is the ratio of post-collision and pre-collision relative velocities of the particles. It is a measure of the amount of energy not dissipated during the collision. For the case of plastic and viscoelastic collision, it is suggested that dissipation should be dependent on impact velocity [11, 13]. The first experimental study on micrometer adhesive polystyrene latex spheres was done by Dahneke [5, 6]. He observed sticking of adhesive particles for low velocities, and increasing coefficient of restitution for velocity higher than a critical threshold. Wall et al. [39], confirmed these results for highly mono-disperse ammonium particles. Both Thornton et al. [31] and Brilliantov et al. [3] presented adhesive visco-elasto-plastic contact models in agreement with these experiments. Work by Sorace et al. [28] further confirms the sticking at low velocities for particles size of the order of a few mm. Li et al [15] proposed a dynamical model based on JKR for the impact of micro-sized spheres with a flat surface. Recently, Brilliantov et al. [27] reported negative coefficients of restitution in nanocluster simulations, which is an artifact of the definition of the coefficient of restitution; one has to relate the relative velocities in the normal directions before and after collision and not just in the frame before collision, which is especially serious for softer particles. Jasevičius et al. [10] have recently presented the

rebound behavior of ultra fine silica particles using the contact model from Refs. [34–36].

We do not review the diverse work involving liquid and solid bridges here, since the focus is on dry particles. Even though oblique collisions between two particles are of practical relevance and have been studied in detail by Thornton et al. [30], here we focus on central normal collisions without loss of generality. We study the dependence of the coefficient of restitution on velocity and material properties, for a wide range of impact velocities, using a modified/generalized version of the contact model by Luding [18], and get consistent results with the previous theoretical and experimental works for low impact velocity. Furthermore, we focus on the less explored intermediate and high velocity regimes, easily accessible in numerical simulations. In the intermediate regime, we observe a similar decreasing trend for the coefficient of restitution, as observed previously [3, 31]. For still increasing impact velocity, we find a second interesting sticking regime due to the contact plastic dissipation. We focus on this regime and present our analysis of two particles collisions with respect to the impact velocity and various material parameters, such as plasticity and adhesion. Moreover, since the physical systems are viscous in nature, we also present some simulations with added viscous damping.

In section 2, we introduce the DEM simulation method and the basic normal contact models as further elaborated on in the following section 3, where the coefficient of restitution is computed. The dependence on adhesivity is described in section 4.2, the effect of viscosity in section 4.3, and some asymptotic solutions in section 4.4, before the study is concluded in section 5.

2 Discrete Element Method

The elementary units of granular materials are mesoscopic grains, which deform under stress. Since the realistic and detailed modeling of real particles in contact is too complicated, it is necessary to relate the interaction force to the overlap δ of two particles. Note that the evaluation of the inter-particle forces based on the overlap may not be sufficient to account for the inhomogeneous stress distribution inside the particles and possible multi-contact effects [11]. This price has to be paid in order to simulate larger samples of particles with a minimal complexity and still taking various physical contact properties like non-linear contact elasticity, plastic deformation or load-dependent adhesion into account.

2.1 Equations of Motion

If all forces acting on a spherical particle p, either from other particles, from boundaries or externally, are known – let their vector sum be f_p – then the problem is reduced to the integration of Newton's equations of motion for the translational degrees of freedom (the rotational degrees are not considered here since we focus on normal forces) for each particle:

$$m_p \frac{\mathrm{d}^2}{\mathrm{d}t^2} r_p = f_p + m_p g \tag{1}$$

where, m_p is the mass of particle p, r_p its position, $f_p = \sum_c f_p^c$ is the total force due to all contacts c, and g is the acceleration due to volume forces like gravity.

With tools from numerical integration, solving the equations of motion, as nicely described in textbooks as [1, 26], is a straightforward exercise. The typically short-ranged interactions in granular media, allow for further optimization by using linked-cell (LC) or alternative methods in order to make the neighborhood search more efficient. However, this is not of concern in this study, since only normal pair collisions are considered.

2.2 Normal Contact Force Laws

Two spherical particles i and j, with radii a_i and a_j, respectively, interact if they are in contact so that their overlap,

$$\delta = (a_i + a_j) - (r_i - r_j) \cdot n \tag{2}$$

is positive, $\delta > 0$, with the unit vector $n = n_{ij} = (r_i - r_j)/|r_i - r_j|$ pointing from j to i. The force on particle i, from particle j, at contact c, can be decomposed into a normal and a tangential part as $f^c := f_i^c = f^n n + f^t t$, where $n \cdot t = 0$. In this paper, we focus on frictionless particles, that is only normal forces will be considered, for tangential forces and torques, see e.g. Ref. [18] and references therein.

In the following, we discuss various normal contact force models, as shown schematically in Fig.1. We start with the linear contact model (Fig.1(a)) for non-adhesive particles, before we introduce a more complex contact model that is able to describe the realistic interaction between adhesive, inhomogeneous, slightly non-spherical particles (Fig.1(b)). In the following (section 2.3) the adhesive non-contact force law will be introduced, while the next section 3 is dedicated to the study of and the computation of the coefficient of restitution.

2.2.1 Linear Normal Contact Model

Modelling a force that leads to an inelastic collision requires at least two ingredients: repulsion and some sort of dissipa-

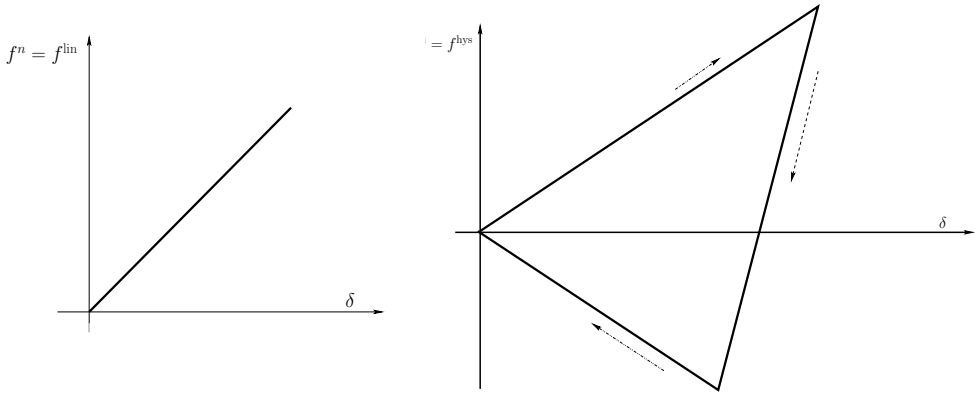

(a) (b)

Fig. 1 Schematic plots of (a) the linear normal contact model for perfectly elastic collision (b) the force-overlap relation for elasto-plastic adhesive collision

tion. The simplest normal force law with the desired properties is the damped harmonic oscillator

$$f^n = k\delta + \gamma_0 v^n \,, \tag{3}$$

with spring stiffness k, viscous damping γ_0, and normal relative velocity $v^n = -v_{ij}\cdot n = -(v_i - v_j)\cdot n = \dot{\delta}$. This model (also called linear spring dashpot (LSD) model) has the advantage that its analytical solution (with initial conditions $\delta(0) = 0$ and $\dot{\delta}(0) = v_i^n$) allows the calculations of important quantities very easily [16]. For the non-viscous case, the linear normal contact model is given schematically in Fig. 1(a).

The typical response time (contact duration) and the eigenfrequency of the contact are related as

$$t_c = \frac{\pi}{\omega} \quad \text{and} \quad \omega = \sqrt{(k/m_r) - \eta_0^2} \tag{4}$$

with the rescaled damping coefficient $\eta_0 = \gamma_0/(2m_r)$, and the reduced mass $m_r = m_i m_j/(m_i + m_j)$. From the solution of the equation of a half-period of the oscillation, one also obtains the coefficient of restitution

$$e_n^{\text{LSD}} = v_f/v_i = \exp(-\pi\eta_0/\omega) = \exp(-\eta_0 t_c) \,, \tag{5}$$

which quantifies the ratio of normal relative velocities after (v_f) and before (v_i) the collision. Note that in this model e_n is independent of v_i. For a more detailed review on this and other, more realistic, non-linear contact models, see [16, 18] and references therein.

The contact duration in Eq. (4) is also of practical technical importance, since the integration of the equations of motion is stable only if the integration time-step Δt is much smaller than t_c. Note that t_c depends on the magnitude of dissipation: In the extreme case of an over-damped spring (high dissipation), t_c can become very large (which renders the contact behavior artificial [20]). Therefore, the use of neither too weak nor too strong viscous dissipation is recommended.

2.2.2 Adhesive Elasto-Plastic Contacts

Here we apply a variation to the piece-wise linear hysteretic model [16–18, 34, 40] as an alternative to non-linear spring-dashpot models or more complex hysteretic models [31, 34–36, 38, 41]. It reflects permanent plastic deformation, which might take place at the contact, and stronger attractive (adhesive) forces, both depending non-linearly on the maximal compression force.

In Fig. 2, the normal force at contact is plotted against the overlap δ between two particles. The force law can be written as

$$f^{\text{hys}} = \begin{cases} k_1\delta & \text{if } k_2(\delta-\delta_0) \geq k_1\delta \\ k_2(\delta-\delta_0) & \text{if } k_1\delta > k_2(\delta-\delta_0) > -k_c\delta \\ -k_c\delta & \text{if } -k_c\delta \geq k_2(\delta-\delta_0) \end{cases} \tag{6}$$

with $k_1 \leq k_2 \leq k_p$, respectively the initial loading stiffness, the un-/re-loading stiffness and the elastic limit stiffness. The latter defines the limit force branch $k_p(\delta - \delta_0^p)$, as will be motivated below in more detail, and k_2 is interpolating between k_1 and k_p, see Eq. (10). For $k_c = 0$, and $k_2 = k_p =$ const., the above contact model reduces to that proposed by Walton and Braun [40], which leads to a constant coefficient of restitution

$$e_n^{\text{WB}} = \sqrt{k_1/k_2^{\text{const.}}} \,, \tag{7}$$

different from the model presented in the following, for which k_2 is *not* a constant.

During the initial loading the force increases linearly with overlap δ along k_1, until the maximum overlap $\delta_{\max} =$

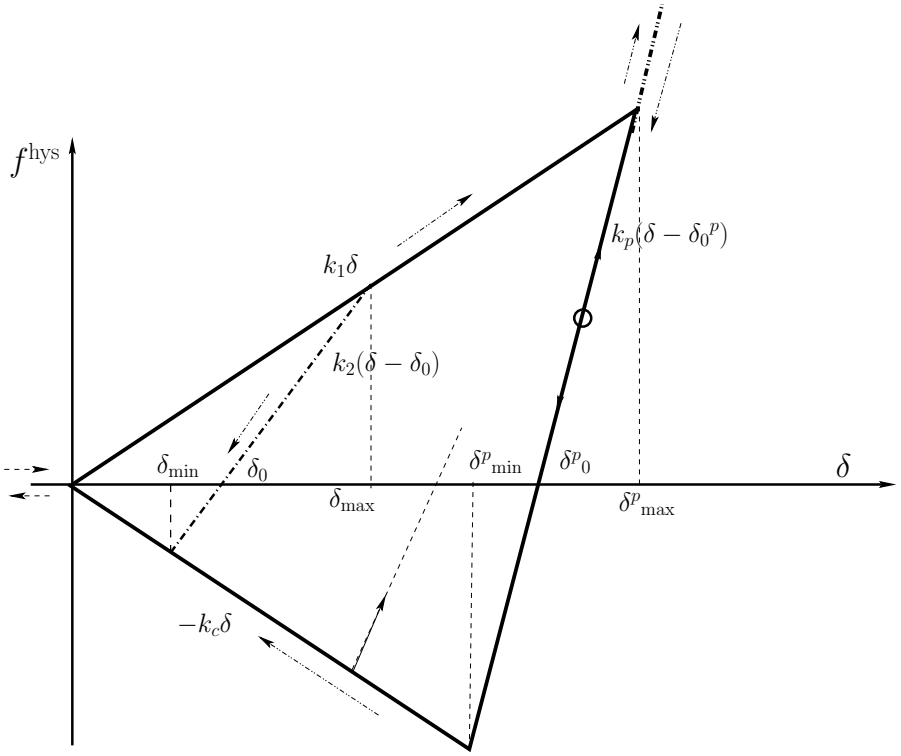

Fig. 2 Schematic graph of the piece-wise linear, hysteretic, and adhesive force-displacement model in normal direction.

$v_i\sqrt{m_r/k_1}$ (for binary collisions) is reached, which is a history parameter for each contact. During unloading the force decreases along k_2, see Eq. (10), from its maximum value $k_1\delta_{\max}$ at $\delta_{\max}$ down to zero at overlap

$$\delta_0 = (1-k_1/k_2)\delta_{\max}\ , \tag{8}$$

where δ_0 resembles the *permanent plastic contact deformation*. Reloading at any instant leads to an increase of the force along the (elastic) branch with slope k_2, until the maximum overlap $\delta_{\max}$ (which was stored in memory) is reached; for still increasing overlap δ, the force again increases with slope k_1 and the history parameter $\delta_{\max}$ has to be updated.

Unloading below δ_0 leads to a negative, *attractive* (adhesive) force, which follows the line with slope k_2, until the extreme adhesive force $-k_c\delta_{\min}$ is reached. The corresponding overlap is

$$\delta_{\min} = \frac{(k_2-k_1)}{(k_2+k_c)}\delta_{\max}\ . \tag{9}$$

Further unloading follows the irreversible tensile branch, with slope $-k_c$, and the attractive force $f^{\mathrm{hys}} = -k_c\delta$.

The lines with slope k_1 and $-k_c$ define the range of possible force values and departure from these lines takes place in the case of unloading and reloading, respectively. Between these two extremes, unloading and reloading follow the line with slope k_2. A non-linear un-/re-loading behavior would be more realistic, however, due to a lack of detailed experimental informations, the piece-wise linear model is used as a compromise; also it is easier to implement. The elastic k_2 branch becomes non-linear and ellipsoidal, when a moderate normal viscous damping force is active at the contact, as in the LSD model.

In order to account for realistic load-dependent contact behavior, the k_2 value is chosen dependent on the maximum overlap $\delta_{\max}$, i.e. *particles are more stiff for larger previous deformation* and dissipation is dependent on deformation. The dependence of k_2 on overlap $\delta_{\max}$ is chosen empirically as linear interpolation:

$$k_2(\delta_{\max}) = \begin{cases} k_p & \text{if } \delta_{\max}/\delta^p_{\max} \geq 1 \\ k_1 + (k_p-k_1)\delta_{\max}/\delta^p_{\max} & \\ & \text{if } \delta_{\max}/\delta^p_{\max} < 1 \end{cases} \tag{10}$$

where k_p is the (maximal) elastic stiffness, and

$$\delta^p_{\max} = \frac{k_p}{k_p-k_1}\phi_f\frac{2a_1a_2}{a_1+a_2}\ , \tag{11}$$

is the plastic flow limit overlap, where ϕ_f represents the dimensionless plasticity depth. From energy balance, one can define the "plastic" limit velocity

$$v_p = \sqrt{k_1/m_r}\,\delta^p_{\max}\ , \tag{12}$$

below which the contact behavior is plastic, and above which it reaches the elastic limit-branch. Impact velocities larger than v_p can have consequences, as discussed next.

2.2.3 Discussion of the adhesive elasto-plastic model

As stated previously, this contact model can be applied to plastic shell-core materials, such as asphalt, ice particles, clusters of fine powders and other fluffy materials: all of them having in common a "soft" plastic outer shell and a rather stiff, elastic inner core. For such materials the stiffness increases with the load due to an increasing contact surface. For higher deformations, contact between the inner cores takes place, which turns out to be almost elastic when compared to the behavior of external shell [25]. Alternatively, the plastic regime can be seen as the range of overlaps, where the surface roughness and inhomogeneities lead to a different contact mechanics as for a more homogeneous inner core. Dissipation on the limit branch – which otherwise would be perfectly elastic – can be taken care of by a linear viscous damping force (as the simplest option). As final remark, for ideal, homogeneous spherical particles, one should refer to other contact models that have a more solid experimental and theoretical foundation [12, 31]

Note that a limit to the slope k_2 that represents *different contact behavior at large deformations* has various other physical and numerical reasons:
(i) in many particle systems, for large deformations the particles cannot be assumed to be spherical anymore, as they deform plastically or even could break;
(ii) from the macroscopic point of view, too large deformations would lead to volume fractions larger than unity, which for most materials (except highly porous plastic ones) would be unaccountable;
(iii) this contact model can also be applied to the case of sintering, see Ref. [22], for large deformation i.e. high temperature, the material goes to a fluid-like state rather than being solid, hence, the elasticity of the system (incompressible melt) determines its limit stiffness;
(iv) at very high values of deformation, the single pair point-contact argument breaks down and multiple contacts of a single particle can not be assumed to be independent anymore;
(v) for more brittle materials, the physics in that regime has to be completely re-considered, since then the particles would fragment/break, which is beyond the scope of the present study;
(vi) numerically, if k_2 would not be limited, the contact duration could become very small so that the minimum time step would have to be reduced below reasonable values.

In summary, the adhesive, elasto- plastic, hysteretic normal contact model is defined by the four parameters k_1, k_p, k_c and ϕ_f that, respectively, account for initial, plastic loading stiffness, maximal, plastic limit (elastic) stiffness, adhesion strength, and plastic overlap-range of the model, with an empirical choice for the interpolated intermediate, nonlinear elastic branch stiffness k_2.

2.3 Non-contact normal force

It has been shown in many studies that long-range interactions are present when dry adhesive particles collide, i.e. forces are present even for negative overlap δ [31]. In the previous section, we have studied the force laws for contact overlap $\delta > 0$, in this section we introduce a description for non-contact, long range, adhesive forces, focusing on the two non-contact models schematically shown in Fig. 3, namely the reversible model and the jump-in (irreversible) model. Later, in the next section, we will combine non-contact and contact forces.

2.3.1 Reversible Adhesive force

In Fig.3(a) we consider the reversible attractive case, where a (linear) van der Waals type long-range adhesive force is assumed. The force law can be written as

$$f^{\text{adh}} = \begin{cases} -f_a & \text{if } \delta > 0 \\ -k_c^a \delta - f_a & \text{if } 0 \geq \delta > \delta_a \\ 0 & \text{if } \delta_a > \delta \end{cases} \tag{13}$$

with the range of interaction $\delta_a = -f_a/k_c^a$, where $k_c^a > 0$ is the adhesive strength of the material and $f_a > 0$ is the (constant) adhesive force magnitude, active for overlap $\delta > 0$ in addition to the contact force. When $\delta = 0$ the force is $-f_a$. The adhesive force f^{adh} is active when particles are closer than δ_a, when it starts increase/decrease linearly along $-k_c^a$, for approach/separation respectively. In the rest of the paper, for the sake of simplicity and without loss of generality, the adhesive strength will be chosen as coincident with the contact adhesive stiffness in Sec. 2.2.2, that is $k_c^a = k_c$.

2.3.2 Jump-in (Irreversible) Adhesive force

In Fig.3(b) we report the behavior of the non-contact force versus overlap when the approach between particles is described by a discontinuous (irreversible) attractive law. The jump-in force can be simply written as

$$f^{\text{jump-in}} = \begin{cases} 0 & \text{if } \delta < 0 \\ -f_a & \text{if } \delta \geq 0 \end{cases} . \tag{14}$$

As suggested in previous studies [3, 12, 31], there is no attractive force before the particles come into contact; the adhesive force becomes active and suddenly drops to a negative value, $-f_a$, at contact, when $\delta = 0$. The jump-in force resembles the limit case $k_c^a \to \infty$ of Eq. (13). Note that the behavior is defined here only for approach of the particles. We assume the model to be irreversible, as in the unloading stage, during separation, the particles will not follow this same path (details will be discussed below).

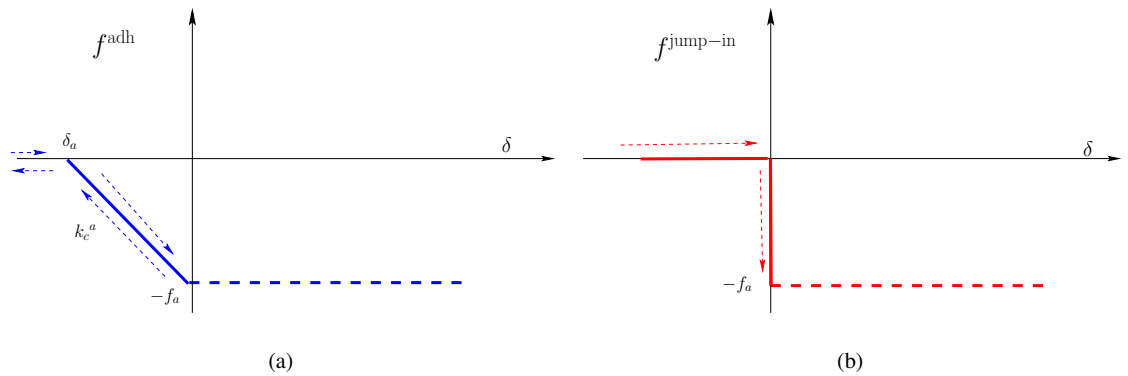

Fig. 3 Schematic plots of (a) the non-contact adhesive force-overlap relation and (b) the non-contact jump-in force-overlap relation.

3 Coefficient of Restitution

As already mentioned, we can quantify the amount of dissipated energy relative to the incident kinetic energy in terms of the coefficient of restitution e, by using the expression $1-e^2$.

When we consider a pair collision, with particles approaching from infinite distance, the coefficient of restitution can be defined as

$$e = \frac{v_f{}^{\infty}}{v_i{}^{\infty}} \tag{15a}$$

and further decomposed as

$$e = \frac{v_f{}^{\infty}}{v_f}\frac{v_f}{v_i}\frac{v_i}{v_i{}^{\infty}} = \varepsilon_o e_n \varepsilon_i \,, \tag{15b}$$

where three different regimes have been introduced to describe the pair interaction. ε_i and ε_o are the pull-in and pull-off coefficients of restitution, that describe the non-contact parts of the interaction ($\delta<0$), for approach and separation of particles respectively, while e_n is the coefficient of restitution defined for particle in contact ($\delta>0$). $v_i\infty$ and $v_f\infty$ denote the approach and separation velocities at infinity distance, when the (short- and long-range) interaction force is zero. v_i is the approaching velocity at zero contact overlap $\delta=0$ (start of contact) and v_f is the separation velocity at zero overlap $\delta=0$ when the particles are separating (end of contact).
In the following, we will first analyze each term in Eq. (15b) separately, based on energy considerations. Then we will show combined contact models using the non-contact and contact components described in sections 2.2-2.3 and provide the coefficient of restitution for this wide class of models.

3.1 Pull-in coefficient of restitution

In order to describe the pull-in coefficient of restitution ε_i we focus on the two non-contact models proposed in Sec. 2.3, as simple interpretations of the adhesive force during the approach of the particles.

When the *reversible adhesive* contact model is used, the energy conservation argument

$$\frac{1}{2}m_r {v_i}^{\infty 2} = \frac{1}{2}f_a\delta_a + \frac{1}{2}m_r {v_i}^2 \tag{16a}$$

yields the following expression for ε_i:

$$\varepsilon_i^{\mathrm{adh}} = \frac{v_i}{v_i{}^{\infty}} = \sqrt{1-\frac{f_a\delta_a}{m_r {v_i}^{\infty 2}}} = \sqrt{1+\frac{f_a^2/k_c}{m_r {v_i}^{\infty 2}}}\,. \tag{16b}$$

The pull-in coefficient of restitution increases with increasing adhesive force magnitude f_a due to increase in attractive force. and decreases with the adhesive strength of the material k_c.

On the other hand, if the *irreversible adhesive jump-in* model is implemented, a constant value $\varepsilon_i^{\mathrm{jump-in}}=1$ is obtained, as $f^{\mathrm{jump-in}}=0$ for $\delta<0$ and the velocity is constant $v_i=v_i{}^{\infty}$.

3.2 Normal coefficient of restitution

When focusing on the contact coefficient of restitution e_n and writing the energy balance between the start and end of contact interaction, we get

$$\frac{1}{2}m_r {v_i}^2 = W_{diss} + \frac{1}{2}m_r {v_f}^2 \tag{17a}$$

and

$$e_n = \frac{v_f}{v_i} = \sqrt{1-\frac{2W_{diss}}{m_r {v_i}^2}}\,, \tag{17b}$$

where W_{diss} denotes the amount of energy dissipated during the collision.

If the *linear* contact model (see Sec. 2.2.1) is considered in the absence of viscous damping (LS), W_{diss} is zero, hence the normal coefficient of restitution $e_n^{\mathrm{LS}} = 1$. On the other hand, for either viscous damping or in the case of *adhesive elasto-plastic* contacts (see Sec 2.2.2), there is finite dissipation. As W_{diss} is always positive, the normal coefficient of restitution is always smaller than unity, i.e. $e^{\mathrm{LSD}} < 1$ and $e_n^{\mathrm{HYS}} < 1$. The coefficient of restitution for the linear spring dashpot model is given in Eq. (5), while the elasto-plastic contact model will be discussed below.

3.3 Pull-off coefficient of restitution

The pull-off coefficient of restitution is defined for particles that lose contact and separate, using the *adhesive reversible* model as described in section 2.3.1. By assuming energy conservation

$$\frac{1}{2}m{v_f}^{\infty 2} = \frac{1}{2}f_a\delta_a + \frac{1}{2}m{v_f}^2 \,, \tag{18a}$$

we obtain the following expression

$$\varepsilon_o = \frac{{v_f}^{\infty}}{v_f} = \sqrt{1+\frac{f_a\delta_a}{m{v_f}^2}} = \sqrt{1-\frac{f_a^2/k_c}{m{v_f}^2}} \,. \tag{18b}$$

Similarly to what already seen for Eq. 16b, the pull-off coefficient of restitution depends on both the adhesive force magnitude f_a and strength k_c, other than the separation velocity v_f. As the particles feel an attractive force during unloading, part of their kinetic energy is lost and hence $\varepsilon_o < 1$ in Eq. (18b).

It is worthwhile to notice that the force-overlap picture described above, with ε_o defined as in Eq. (18b) refers to a system with sufficiently high impact velocity, so that the particles can separate with a finite kinetic energy at the end of collision. That is

$${v_f}^2 > f_a^2/(mk_c) =: (v_f^a)^2 \tag{19}$$

or, equivalently, $v_i^{\infty} > v_f^a/(e_n\varepsilon_i)$, where v_f^a denotes the maximum relative velocity at which particles actually can separate. On the other hand, if the kinetic energy reaches zero before the separation, e.g. during the unloading path, the particles start re-loading along the adhesive branch until the value $\delta = 0$ is reached and they follow contact law defined for $\delta > 0$ again.

3.4 Combined contact laws

The contact and non-contact models described in previous sections 3.1, 3.2 and 3.3 can be combined in order to obtain the overall description of the system behavior, during approach, contact and final separation of the particles.

For example, the combination of the pull-in, the linear normal and the pull-off components leads to a *reversible adhesive linear* contact model, as shown schematically in the upper part of Fig. 4(a), with coefficient of restitution $e = \varepsilon_o e_n^{\mathrm{LSD}} \varepsilon_i^{\mathrm{adh}}$. On the other hand, by combining the irreversible (jump-in) pull-in, the linear normal and the (reversible) pull-off components (see schematic in the lower part of Fig. 4(a)) we get coefficient of restitution $e = \varepsilon_o e_n^{\mathrm{LSD}} \varepsilon_i^{\mathrm{jump-in}}$.

In the following we will focus on the combination of the irreversible pull-in with the adhesive elasto-plastic and the (reversible) pull-off parts, leading to an *irreversible adhesive elasto-plastic* model, see Fig. 4(b), with $e = \varepsilon_o e_n^{\mathrm{HYS}} \varepsilon_i^{\mathrm{jump-in}} = \varepsilon_o e_n^{\mathrm{HYS}}$. For this special case we want to analyze the influence of the adhesive component/parameters on the overall behavior.

In Fig. 5, we plot the coefficient of restitution e. as a function of impact velocity for both the irreversible elastic ($e_n = e_n^{\mathrm{LSD}}$) and the irreversible elasto-plastic ($e_n = e_n^{\mathrm{HYS}}$) contact models. We observe that for low velocity the system behaves in a similar fashion in both cases, showing an initial sticking regime, in agreement with previous experimental and numerical results [28, 31, 39] At higher velocities, a significant difference appears: for elastic adhesive spheres, e keeps increasing and approaches unity while, for elasto-plastic adhesive spheres, e starts decreasing at intermediate velocity until it becomes zero at higher velocity. This difference is related with the sources of dissipation in the two models. In the irreversible elastic case, energy is dissipated only due to the pull-off of the particles, which is significant in low velocity range only. On the contrary, for irreversible elasto-plastic spheres, dissipation takes place during both, pull-off and normal contact, stages. The latter, new, effect is negligible for low velocity (hence the two models coincide) but it becomes important for large impact velocity, leading to a second, high velocity, sticking regime, (that will be discussed in detail below).

Furthermore, in Fig. 6, we focus on the strength of the non-contact adhesion f_a and we plot e against the impact velocity for different f_a. We observe that for $f_a = 0$, $e_n \approx 1$ at low velocities, while, for finite f_a, the particles stick to each other with $e_n = 0$. The critical velocity v_f^a required to separate the particles increases with f_a. For extreme values of f_a the particles stick in the whole range of velocities.

It is interesting to notice that for very low f_a and low impact velocities the behavior is independent of the adhesive force magnitude (cyan line and black circles lie on top of each other in Fig. 6). In the further sections we restrict our analysis to this range of f_a and impact velocity, as almost all practical collision take place in this range.

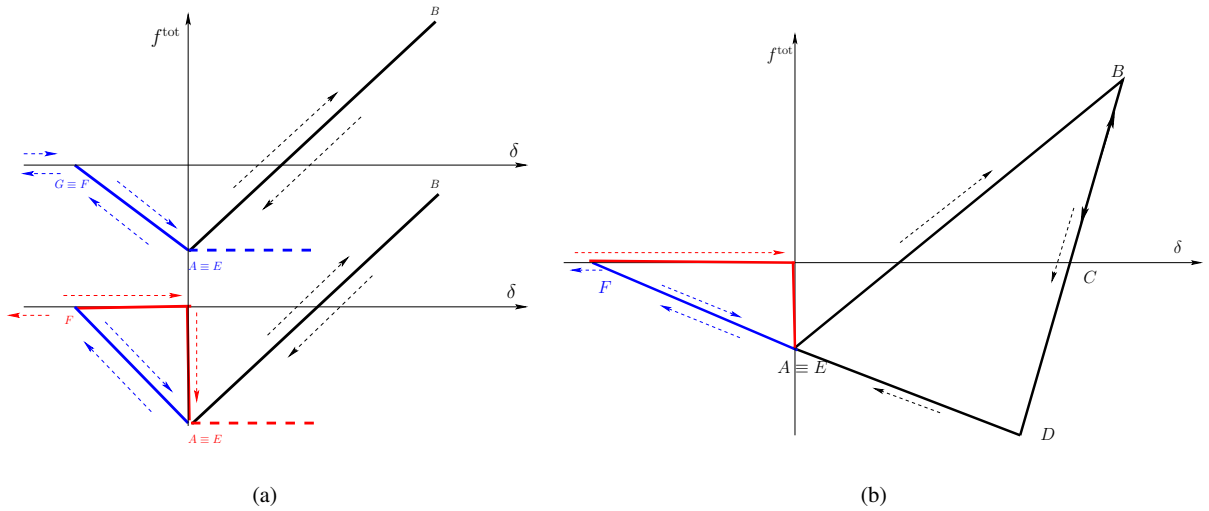

Fig. 4 (a) Reversible and irreversible non-contact forces, where the top blue line (for negative overlap) represents the former and the bottom red line (for negative overlap) the latter. The black line for positive overlap represents the linear contact force as superimposed on the non-contact force. (b) Force-displacement law for elasto-plastic, adhesive contacts superimposed on the irreversible non-contact adhesive force.

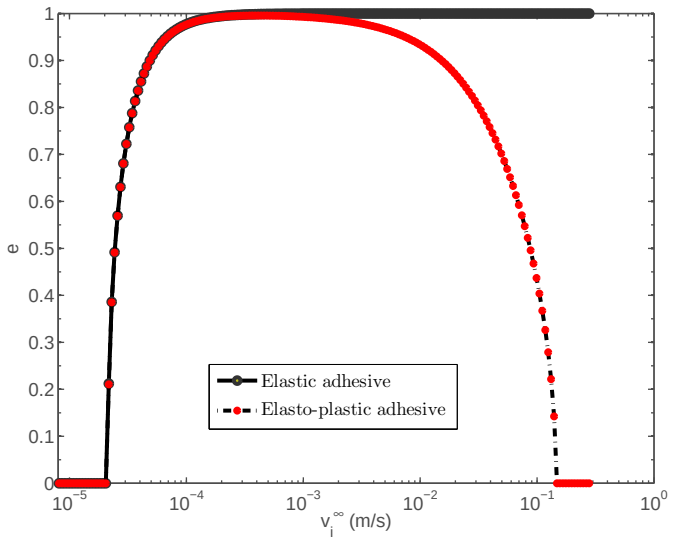

Fig. 5 Restitution coefficient e plotted as a function of the impact velocity v_i^∞ $e_n - > e$ and $v_i - > v_i^\infty$ for irreversible elastic-adhesive and elasto-plastic adhesive spheres (as given in the inset). Parameters used here are $k_1 = 10^2\,\mathrm{Nm}^{-1}$, $k_p = 5\times10^2\,\mathrm{Nm}^{-1}$, $k_c = 10^2\,\mathrm{Nm}^{-1}$, and $f_a = 5\times10^{-7}\,\mathrm{N}$, which leads to the low-velocity sticking limit $v_f^a = 2.1\times10^{-5} m/s$, for particles with radius $1.1.10^{-3}$ m, density $2000\,\mathrm{kg/m}^3$, and mass $m = 5.6\times10^{-6}\,\mathrm{kg}$.

4 Elasto-plastic coefficient of restitution

In the following we will restrict our analytical study on the coefficient of restitution to the range of moderate and large impact velocity, where the contribution of weak non-contact adhesive forces $f_a \to 0$ can be neglected. Furthermore, we disregard viscous forces in order to allow for a closed analytical treatment. The coefficient of restitution will be computed and its dependence on the impact velocity v_i and the adhesive stiffness k_c is considered for two cases $v_i < v_p$ and $v_i \geqslant v_p$, with v_p defined in Eq. (12).

4.1 Theory and dimensionless parameters

4.1.1 Initial relative velocity $v_i < v_p$

When $v_i < v_p$ the particles after loading, unload with slope k_2 and the system deforms along the path $0 \to \delta_{\max} \to \delta_0 \to \delta_{\min} \to 0$, as described in the Sec. 2.2.2 and shown in Fig. 2.

The initial kinetic energy (at $\delta = 0$ overlap) is completely transformed to potential energy at the maximum over-

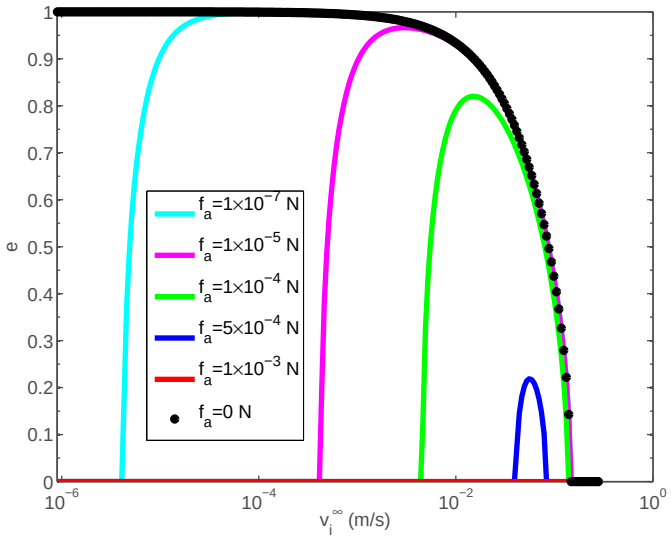

Fig. 6 Restitution coefficient plotted as function of impact velocity. Different lines correspond to the analytical expression in Eq. (26) with different f_a as given in the inset. Black circles represent the numerical solution results for $f_a = 0$, where parameters are the same as in Fig. 5.

lap $\delta_{\max}$,

$$\frac{1}{2}m_r v_i^2 = \frac{1}{2}k_1\delta_{\max}^2 \ . \tag{20a}$$

The direction of relative velocity is reversed at $\delta_{\max}$, unloading starts with slope k_2 and some part of the potential energy is converted to kinetic energy at the force-free overlap δ_0,

$$\frac{1}{2}m_r v_0^2 = \frac{1}{2}k_2(\delta_{\max}-\delta_0)^2 \ , \tag{20b}$$

which, using Eq. (8), can be written as

$$\frac{1}{2}m_r v_0^2 = \frac{1}{2}k_1\delta_{\max}(\delta_{\max}-\delta_0) \ . \tag{20c}$$

Further unloading, below δ_0, leads to attractive forces. The kinetic energy at δ_0 is partly converted to potential energy at $\delta_{\min}$

$$\frac{1}{2}m_r v_{\min}^2 + \frac{1}{2}k_2(\delta_{\min}-\delta_0)^2 = \frac{1}{2}m_r v_0^2 \ . \tag{20d}$$

The total energy is finally converted to only kinetic energy at the end of the collision (overlap $\delta = 0$)

$$\frac{1}{2}m_r v_f^2 - \frac{1}{2}m_r v_{\min}^2 = -\frac{1}{2}k_c\delta_{\min}^2 \ , \tag{20e}$$

that, when combined with (20d), gives

$$\frac{1}{2}m_r v_f^2 - \frac{1}{2}m_r v_0^2 = -\frac{1}{2}k_c\delta_{\min}\delta_0 \tag{20f}$$

Using Eqs. (20a), (20c), and (20f) with the definitions of $\delta_{\min}$ and δ_0, and dividing by the initial kinetic energy, we obtain the coefficient of restitution

$$e_n^{(1)} = \frac{v_f}{v_i} = \sqrt{\frac{k_1}{k_2} - \frac{k_c}{k_1}\frac{(k_2-k_1)}{(k_2+k_c)}\frac{(k_2-k_1)}{k_2}} \tag{21}$$

with $k_2 = k_2(\delta_{\max}) = k_2(v_i)$, as defined in Eq. (10).

4.1.2 Initial relative velocity $v_i \geqslant v_p$

When the initial relative velocity v_i is large enough such that $v_i \geqslant v_p$, the estimated maximum overlap $\delta_{\max} = v_i\sqrt{m_r/k_1}$ is greater than $\delta_{\max}^p$. Let v_1 be the velocity at overlap $\delta_{\max}^p$. The system deforms along the path $0 \to \delta_{\max}^p \to \delta_{\max} \to \delta_0 \to \delta_{\min} \to 0$, see Fig. 2. The initial relative kinetic energy is not completely converted to potential energy at $\delta = \delta_{\max}^p$, hence

$$\frac{1}{2}m_r v_i^2 = \frac{1}{2}m_r v_1^2 + \frac{1}{2}k_1(\delta_{\max}^p)^2, \tag{22a}$$

and the loading continues with the slope k_p until all kinetic energy equals zero at $\delta = \delta_{\max} > \delta_{\max}^p$

$$\frac{1}{2}m_r v_1^2 + \frac{1}{2}k_1(\delta_{\max}^p)^2 = \frac{1}{2}k_p(\delta_{\max}-\delta_0)^2, \tag{22b}$$

the relative velocity changes sign at $\delta_{\max}$, the contact starts to unload with slope k_p. The potential energy is completely converted to kinetic energy at δ_0, such that the equality

$$\frac{1}{2}m_r v_0^2 = \frac{1}{2}k_p(\delta_{\max}-\delta_0)^2 \tag{22c}$$

or

$$\frac{1}{2}m_r v_0^2 = \frac{1}{2}k_1\delta_{\max}^p(\delta_{\max}^p-\delta_0) + \frac{1}{2}m_r v_1^2 \tag{22d}$$

holds. Further unloading, still with slope k_p, leads to attractive forces until $\delta_{\min}^p$ is reached, where the kinetic energy is partly converted to potential energy

$$\frac{1}{2}m_r v_{\min}^2 + \frac{1}{2}k_p(\delta_{\min}^p-\delta_0)^2 = \frac{1}{2}m_r v_0^2 \ . \tag{22e}$$

The unloading continues along k_c and the total energy at $\delta^p_{\min}$ is finally converted to only kinetic energy at the end of collision ($\delta = 0$ overlap), so that

$$\frac{1}{2}m_r v_f^2 - \frac{1}{2}m_r v_{\min}^2 = -\frac{1}{2}k_c(\delta^p_{\min})^2 \,. \tag{22f}$$

Using Eqs. (22c) and (22d) in Eq. (22f) gives

$$\frac{1}{2}m_r v_f^2 - \frac{1}{2}m_r v_0^2 = -\frac{1}{2}k_c\delta^p_{\min}\delta_0 \,. \tag{22g}$$

Combining Eqs. (22a), (22b), (22c), (22g) with the definitions of $\delta^p_{\min}$ and δ_0, and dividing by the initial kinetic energy, we obtain the coefficient of restitution

$$e_n^{(2)} = \sqrt{1 + \left[-1 + \frac{k_1}{k_p} - \frac{k_c}{k_1}\frac{(k_p-k_1)^2}{(k_p+k_c)k_p}\right]\frac{v_p^2}{v_i^2}} \,, \tag{23}$$

with $v_p/v_i < 1$.

4.1.3 Dimensionless Parameters

For a more general description, a few dimensionless parameters can be defined:

$$\text{Plasticity} : \eta = \frac{k_p - k_1}{k_1} \,, \tag{24a}$$

$$\text{Adhesivity} : \beta = \frac{k_c}{k_1} \,, \tag{24b}$$

$$\text{Scaled initial velocity} : \chi = \frac{\delta_{\max}}{\delta^p_{\max}} \sim \frac{v_i}{v_p} \,. \tag{24c}$$

The final dimensionless number, given here for the sake of completeness, but not used in this subsection, is the ratio of maximum velocity at which particles stick due to adhesion only to the initial relative velocity of the particles. $\psi_a = v_a/v_i^\infty \ll 1$.

Using Eqs. (24a), (24b) and (24c) in Eq. (10), one can define

$$k_2(\chi) = \begin{cases} k_p & \text{if } \chi \geq 1 \\ k_1(1+\eta\chi) & \text{if } \chi < 1 \end{cases} \,, \tag{25}$$

while the coefficients of restitution, $e_n^{(1)}$ in Eq. (21) and $e_n^{(2)}$ in Eq. (23) become

$$e_n^{(1)}(\eta,\beta,\chi<1) = \sqrt{\frac{1}{1+\eta\chi} - \frac{\beta\eta^2\chi^2}{(1+\eta\chi)(1+\beta+\eta\chi)}} \tag{26}$$

and

$$e_n^{(2)}(\eta,\beta,\chi\geq 1) = \sqrt{1 + [A(\eta,\beta)-1]\,\frac{1}{\chi^2}} \,, \tag{27}$$

with

$$A(\eta,\beta) = \left[e_n^{(1)}(\eta,\beta,\chi=1)\right]^2 \,. \tag{28}$$

4.1.4 Qualitative Description

In Fig. 7, the analytical prediction for the coefficient of restitution, from Eqs. (26) and (27), is compared to the numerical integration of the contact model, for different scaled initial velocities χ. In the whole range, we confirm the validity of the theoretical prediction for the coefficient of restitution.

For very small $\eta\chi < 10^{-3}$, e_n can be approximated as $e_n^{(1)} \approx 1 - \frac{\eta\chi}{2}$. With increasing initial relative velocity v_i, dissipation increases faster than the initial kinetic energy and leads consequently, to a faster convex decrease of $e_n^{(1)}$. The coefficient of restitution $e_n^{(1)}$ becomes zero when a critical scaled initial velocity $\chi_c^{(1)}$ (see Eq. (30) below) is reached. At this point, the amount of dissipated energy is equal to the initial kinetic energy, making the particles stick to each other. The coefficient of restitution stays zero up to a second critical scaled initial velocity $\chi_c^{(2)}$ is reached, i.e. one has sticking for $\chi_c^{(1)} \leq \chi \leq \chi_c^{(2)}$. Finally for scaled initial velocities $\chi > \chi_c^{(2)}$, the dissipated energy remains constant (plastic limit is reached), while the initial kinetic energy increases. As a result, the kinetic energy after collision increases and so does the coefficient of restitution e_n. [1]

In Fig. 8, we compare the variation of the force with overlap in the various regimes of χ as discussed above. For very small χ, the unloading slope $k_2 \approx k_1$, (see Fig. 8(a) for a moderately small $\chi = 0.34$), and the amount of dissipated energy is small, increasing with χ. The kinetic energy after collision is almost equal to the initial kinetic energy, i.e. $e_n \sim 1$, see Fig. 7. In Figs. 8(b) and 8(c), the force-overlap variation is shown for sticking particles, for the cases $\chi_c^{(1)} < \chi < 1$ and $1 < \chi < \chi_c^{(2)}$, respectively (more details will be given in the following subsection). Finally, in Fig. 8(d), the case $\chi > \chi_c^{(2)}$ is displayed, for which the initial kinetic energy is larger than the dissipation, resulting in the separation of the particles. The corresponding energy variation is described in detail in the appendix.

4.1.5 Sticking regime limits and overlaps

In this section we focus on the range of $\chi_c^{(1)} < \chi \leq \chi_c^{(2)}$, where the particles stick to each other and calculate the critical values $\chi_c^{(1)}$ and $\chi_c^{(2)}$. Also we assume β to be large enough so that sticking is possible, as we show in later section that for a given η a minimum $\beta = \beta^*$ is required for particles to stick. When $\chi = \chi_c^{(1)}$ all initial kinetic energy of the particles is dissipated during the collision. Hence the particles stick and e_n becomes zero:

$$e_n^{(1)}(\eta,\beta,\chi_c^{(1)}) = 0 \,, \tag{29a}$$

[1] Note that this is the regime where the physics of the contact changes and dependent on the material and other considerations, modifications to the contact model could/should be applied, however, this goes beyond the scope of this paper.

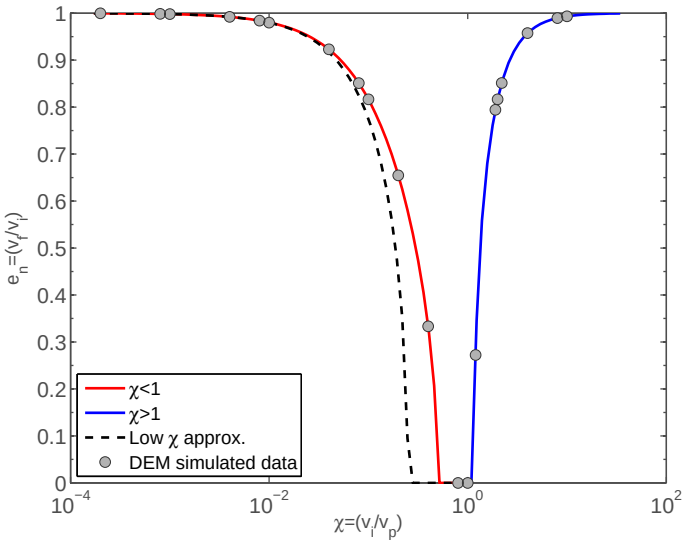

Fig. 7 Restitution coefficient plotted as a function of the scaled initial velocity χ. The lines correspond to the analytical expressions in Eqs. (26) and (27), for the two regimes, and circles are DEM simulations, while the dashed line represents the low velocity approximation results for the same material parameters as in Fig. 5, i.e. $\eta = 4$ and $\beta = 1$.

which leads to

$$\beta\eta^2\chi^2 - \eta\chi - (1+\beta) = 0\,. \tag{29b}$$

Only the positive χ solution is physically possible, as particles with negative initial relative velocity cannot collide, so that

$$\chi_c^{(1)} = \frac{1}{2\beta\eta}\left[1+\sqrt{1+4\beta(1+\beta)}\right]\,. \tag{30}$$

For larger $\chi > \chi_c^{(1)}$, the dissipation is strong enough to consume all the initial kinetic energy, hence the particles loose kinetic energy at a positive, finite overlap δ_c, see Fig. 8(b). The contact deforms along the path $0 \to \delta_{max} \to \delta_0 \to \delta_{min} \to \delta_c$. Thereafter, in the absence of other sources of dissipation, particles keep oscillating along the same slope k_2. In order to compute δ_c, we use the energy balance relations in Eqs. (20), and conservation of energy along $\delta_{min} \to \delta_c$, as described by Eq. (20e)

$$\frac{1}{2}m_r v_f^2 - \frac{1}{2}m_r v_0^2 = -\frac{1}{2}k_c\left\{\delta_{min}\delta_0 - \frac{1}{2}k_c\delta_c^2\right\}\,, \tag{31a}$$

with $v_f = 0$ at the overlap δ_c. Re-writing in terms of k_c and δ_{max} leads to

$$k_c\delta_c^2 + \left\{\frac{k_1^2}{k_2} - \frac{k_c(k_2-k_1)^2}{k_2(k_2+k_c)}\right\}\delta_{max}^2 = 0 \tag{31b}$$

and thus to the sticking overlap

$$\frac{\delta_c^{(1)}}{\delta_{max}^p} = \frac{\delta_{max}}{\delta_{max}^p}\sqrt{\frac{(k_2-k_1)^2}{k_2(k_2+k_c)} - \frac{k_1^2}{k_2k_c}}\,. \tag{31c}$$

In terms of dimensionless parameters, as defined earlier, one gets

$$\frac{\delta_c^{(1)}}{\delta_{max}^p} = \chi\sqrt{\frac{\eta^2\chi^2}{(1+\eta\chi)(1+\beta+\eta\chi)} - \frac{1}{\beta(1+\eta\chi)}} = \frac{\chi}{\sqrt{\beta}}|e_n^{(1)}|\,, \tag{32}$$

where $|e_n^{(1)}|$ denotes the absolute value of the result from Eq. (26)

For larger initial relative velocities, $\chi \geq 1$, the coefficient of restitution is given by Eq. (27), so that the second critical $1 < \chi_c^{(2)}$ can be computed setting

$$e_n^{(2)}(\eta,\beta,\chi_c^{(2)}) = 0\,, \tag{33a}$$

or

$$\left[\frac{1}{1+\eta} - \frac{\beta\eta^2}{(1+\eta)(1+\beta+\eta)} - 1\right]\frac{1}{\chi^2} = 1\,. \tag{33b}$$

Again, only the positive solution is physically possible, so that

$$\chi_c^{(2)} = \sqrt{1 - \frac{1}{1+\eta} + \frac{\beta\eta^2}{(1+\eta)(1+\beta+\eta)}} \tag{34}$$

is the maximum value of χ for which particles stick to each other. For $\chi \leqslant \chi_c^{(2)}$ particles deform along the path $0 \to \delta_{max}^p \to \delta_{max} \to \delta_0 \to \delta_{min} \to \delta_c$ and then keep oscillating with k_2 stiffness, δ_c being one of the extrema of the oscillation, see Fig. 8(c). From Eq. (22e), applying conservation of energy along $\delta_{min} \to \delta_c$, we get

$$\frac{1}{2}m_r v_f^2 - \frac{1}{2}m_r v_0^2 = -\frac{1}{2}k_c\delta_{min}\delta_0 + \frac{1}{2}k_c\delta_c^2\,, \tag{35a}$$

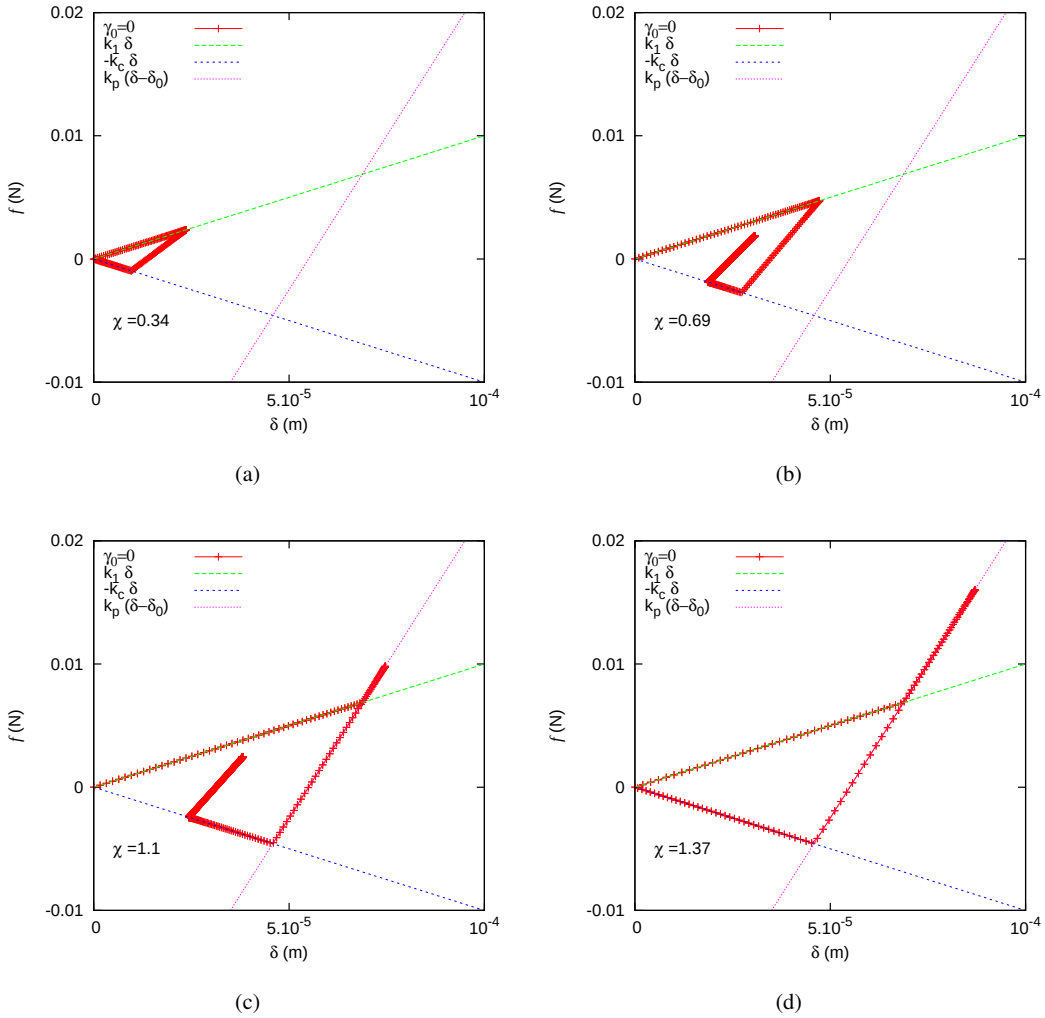

Fig. 8 Contact force during one collision, plotted against the overlap for different scaled initial velocities $\chi = 0.34, 0.69, 1.1$, and 1.37, respectively. The three straight lines represent the plastic branch, with slope k_1, the adhesive branch, with slope $-k_c$, and the limit branch with slope k_p, for $k_1 = 10^2\ \mathrm{Nm}^{-1}$, $k_p = 5 \times 10^2\ \mathrm{Nm}^{-1}$ and $k_c = 10^2\ \mathrm{Nm}^{-1}$, i.e. $\eta = 4$ and $\beta = 1$

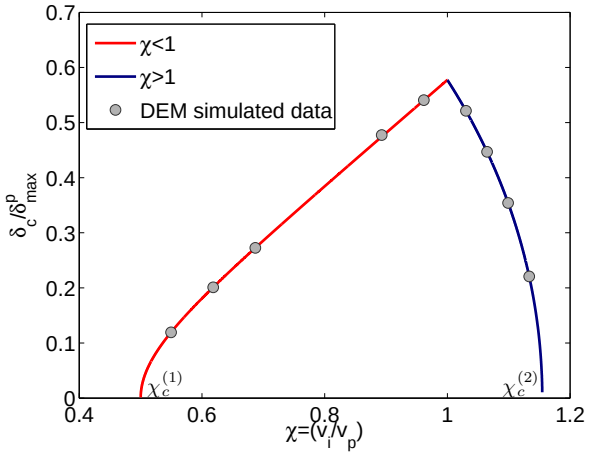

Fig. 9 Kinetic energy-free contact overlap δ_c plotted as a function of the scaled initial velocity $\chi = \frac{v_i}{v_p}$; the increasing branch corresponds to $\chi < 1$, while the decreasing branch corresponds to $\chi > 1$. The dots are simulations for $\eta = 4$ and $\beta = 1$, as in Fig. 8, which yields $\delta_c^{\max}/\delta_{\max}^{p} = (1/3)^{1/2}$ in Eq. (37).

with $v_f = 0$, and re-writing in terms of k_c and $\delta^p_{\max}$ leads to

$$\frac{\delta_c^{(2)}}{\delta^p_{\max}} = \sqrt{\left[\frac{(k_p-k_1)^2}{k_p(k_p+k_c)} - \frac{k_1^2}{k_c k_p} + \frac{k_1}{k_c}\right] - \frac{m_r}{k_c}\frac{v_i^2}{(\delta^p_{\max})^2}} \,. \tag{35b}$$

In terms of the dimensionless parameters, this yields

$$\frac{\delta_c^{(2)}}{\delta^p_{\max}} = \sqrt{\frac{\eta^2}{(1+\eta)(1+\beta+\eta)} + \frac{\eta}{\beta(1+\eta)} - \frac{\chi^2}{\beta}} = \frac{\chi}{\sqrt{\beta}}|e_n^{(2)}| \,, \tag{36}$$

where $|e_n^{(2)}|$ denotes the absolute value of the result from Eq. (27)

In Fig. 9, the evolution of $\delta_c/\delta^p_{\max}$ with χ is reported, showing perfect agreement of the analytical expressions in Eqs. (32) and (36), with the numerical solution of a pair-collision. In the sticking regime, the stopping overlap increases with χ, and reaches a maximum at $\chi = 1$,

$$\delta_c^{\max}/\delta^p_{\max} = \sqrt{\frac{\beta\eta^2 - \eta - \beta - 1}{\beta(1+\eta)(1+\eta+\beta)}} \tag{37}$$

which depends on the the adhesivity β and the plasticity η only. For $\chi > 1$, dissipation gets weaker, relatively to the increasing initial kinetic energy, and $\delta_c^{(2)}/\delta^p_{\max}$ decreases. until it reaches 0 for $\chi = \chi_c^{(2)}$.

4.2 Dependence on Adhesivity β

In the previous subsections, we studied the dependence of the coefficient of restitution e_n on the scaled initial velocity χ for fixed adhesivity β, whereas here the dependence of e_n on β is analyzed.

A special adhesivity β^* can be calculated such that $e_n = 0$ for $\chi = 1$, which is the case of maximum dissipation and leads to sticking only at exactly $\chi = 1$. From Eq. (26), we get

$$1 + \beta^* + \eta - \beta^*\eta^2 = 0 \,, \tag{38a}$$

so that

$$\beta^* = \frac{1}{\eta - 1} \,. \tag{38b}$$

In Fig. 10, we plot the coefficient of restitution as function of the scaled initial velocity χ for different values of adhesivity β. For $\beta < \beta^*$, in Fig. 10, the coefficient of restitution e_n decreases with increasing $\chi < 1$, reaches its positive minimum at $\chi = 1$, and increases for $\chi > 1$. In this range, the particles (after collision) always have a non-zero relative separation velocity v_f. When $\beta = \beta^*$, e_n follows a similar trend, becomes zero at $\chi = 1$, and increases with increasing scaled initial velocity for $\chi > 1$. This is the minimum value of adhesivity for which e_n can become zero and particles start to stick to each other. For $\beta = \beta^*$, the two critical values coincide, $\chi_c^{(1)} = \chi_c^{(2)} = 1$. If $\beta > \beta^*$, e_n decreases and becomes zero at $\chi = \chi_c^{(1)} < 1$, it remains zero until $\chi = \chi_c^{(2)} > 1$, and from there increases with increasing initial velocity.

4.3 Effect of Viscosity

Since real physical systems also can have additional dissipation modes that are, e.g., viscous in nature, in this section we study the behavior of the collision when viscosity is present ($\gamma_0 > 0$) and compare it with the non-viscous case ($\gamma_0 = 0$). Note that any non-linear viscous damping force can be added to the contact laws introduced previously, however, for the sake of simplicity we restrict ourselves to the simplest linear viscous law as given as second term in Eq. (3). In Fig. 11, we plot the contact force against the overlap, and the overlap against time, during collisions for a constant value of $\chi = 1$ and different β, for $\gamma_0 = 5 \times 10^{-3}$.

When $\beta < \beta^*$, see Fig. 11(a) and Fig. 11(b), the contact ends when the adhesive force $-k_c\delta$ goes back to zero, for both cases, with and without viscosity. This is since the viscosity is relatively small and does not contribute enough to the total dissipation to make the particles stick.

For the critical adhesivity $\beta = \beta^*$, reported in Fig. 11(c), without viscosity the overlap between the particles still goes down to exactly zero at the end of the collision, with all kinetic energy dissipated. For $\gamma_0 > 0$, dissipation brings this marginal collision case into the sticking regime and the particles stay in contact at $\delta > 0$. This can be seen clearly in Fig. 11(d), where the particles undergo a damped oscillatory motion with amplitude depending on the residual velocity v_f (the amplitude is very small due to small residual velocity).

For larger values $\beta > \beta^*$, the overlap does not reach 0, neither for $\gamma_0 = 0$ nor for $\gamma_0 > 0$, see Fig. 11(e). In both cases, the particles stick and remain in contact with a finite overlap. Without viscosity, the particles keep oscillating along the slope k_2, while in the case with viscosity the oscillation is damped and kinetic energy vanishes. During loading and unloading the apparent slope changes with time due to the additional viscous force that leads to the dissipation of energy. Waiting long enough, for some oscillation cycles, the particles stick to each other with a finite overlap and zero relative kinetic energy. The difference is displayed in Fig. 11(f), where for $\gamma_0 = 0$ the particles keep oscillating with constant amplitude, whereas, for $\gamma_0 > 0$, the particles undergo a damped oscillatory motion, until the velocity becomes 0 at $\delta > 0$. The time evolution of the overlap in Fig. 11(f) resembles that of the displacement evolution in

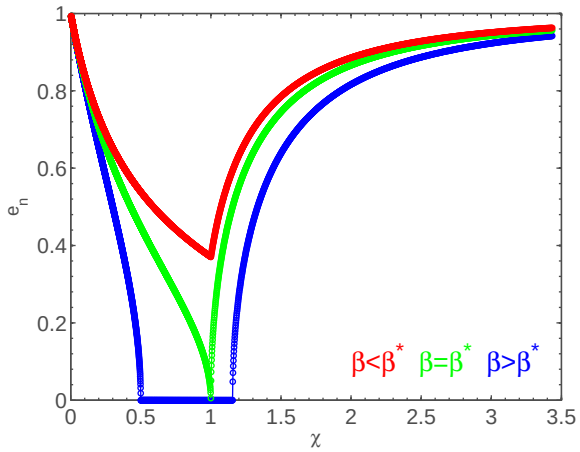

Fig. 10 Coefficient of restitution e_n plotted against the scaled initial velocity χ. Different colors correspond to different adhesivity β (red for $\beta < \beta^*$, green for $\beta = \beta^*$ and blue for $\beta > \beta^*$), with parameters $k_1 = 10^2$, $k_p = 5 \times 10^2$, and different k_c (all in units of Nm^{-1}), i.e. $\eta = 4$ and $\beta/\beta^* = 1/3$, 1, and 3, with $\beta^* = 1/3$.

Ref. [8], where the authors studied sticking of particles in Saturn's rings. [2]

4.4 Asymptotic Solutions

In this subsection, we focus on the case $\chi \leq 1$, and study the asymptotic behavior of the coefficient of restitution as function of the impact velocity.

For the sake of simplicity, let us start with an elasto-plastic system without adhesion, i.e. $k_c = 0$, in Eq. (26) such that

$$e_n^{(1)}(\eta, \beta = 0, \chi < 1) = \sqrt{\frac{1}{1+\eta\chi}} \approx (\eta\chi)^{-1/2} \tag{39}$$

with the approximation valid for $\eta\chi \gg 1$. Since the scaled velocity is moderate, $\chi < 1$, the condition requires a large plasticity, i.e., a strong difference between the limit stiffness and the plastic loading stiffness, $\eta \gg 1$ (or $k_p \gg k_1$). In Fig. 12, we plot the coefficient of restitution against the scaled initial velocity χ for three different values of $\eta = k_p/k_1$, together with the power law prediction of Eq. (39). We observe, that for the smallest η (red circle and line), the approximation is far from the data, while for higher η, the approximation works well even for rather small velocities $\chi \approx 0.1$.

Next, when studying the elasto-plastic adhesive contact model, $\beta > 0$ and $\beta \ll 1$, again, we restrict ourselves to values of η such that asymptotic condition $\eta\chi \gg 1$ is satisfied. Hence, Eq. (26) can be approximated as

$$e_n^{(1)}(\eta, \beta, \chi < 1) \approx \sqrt{\frac{1}{\eta\chi} - \beta}\,, \tag{40}$$

as long as $\eta\chi \gg \beta \geq 0$ and $\frac{1}{\eta} > \beta$ holds.

In Fig. 13, we plot the coefficient of restitution against the scaled initial velocity χ for different values of β and superimpose the approximation, Eq. (40). For small β and large χ, one observes good agreement between the full solution and the approximation. Differently, for the highest values of β the approximation is not valid. Due to the adhesive force, for large χ, with increasing β, the deviation from the $\chi^{-1/2}$ power law becomes stronger and stronger, leading to the sticking regime, as discussed in the previous subsections. On the other hand, for smaller velocities, one observes a considerably smaller power-law, resembling the well-known $\chi^{-1/4}$ power law for plastic contacts, as indicated by the dashed line in Fig. 13.

4.5 Dependence on interpolation

The choice of the interpolation rule for the unloading stiffness k_2 in Eq. (25) is empirical. Therefore, for $\delta_{\max}/\delta^p_{\max} < 1$, a different choice could be:

$$k_2(\delta_{\max}) = k_1(1 + \eta\sqrt{\chi}) \tag{41}$$

Inserting Eq. (41) into Eq. (21) leads to a different expression for the normal coefficient of restitution $e_n^{(1)}$, which for high values of $\eta\sqrt{\chi}$, and for small β, reduces to

$$e_n \propto \sqrt{\eta}(\chi)^{-1/4}\,. \tag{42}$$

A similar power law prediction for moderate velocities has been previously obtained by Thornton et al. in Ref. [31], using a non-linear Hertzian loading and unloading. Fig. 14 shows the agreement between the power law approximation $\chi^{-1/4}$ and Eq. (21) with the alternative interpolation rule (41), for moderate velocities. The choice of different interpolation laws for k_2 shows the flexibility of the model and requires input from experiments to become more realistic.

[2] In general, one could add a viscous law that is proportional to $k_2 - k_1$ such that the jump-in viscous force in (e) at the beginning of the contact is not there, however, we do not go into this detail.

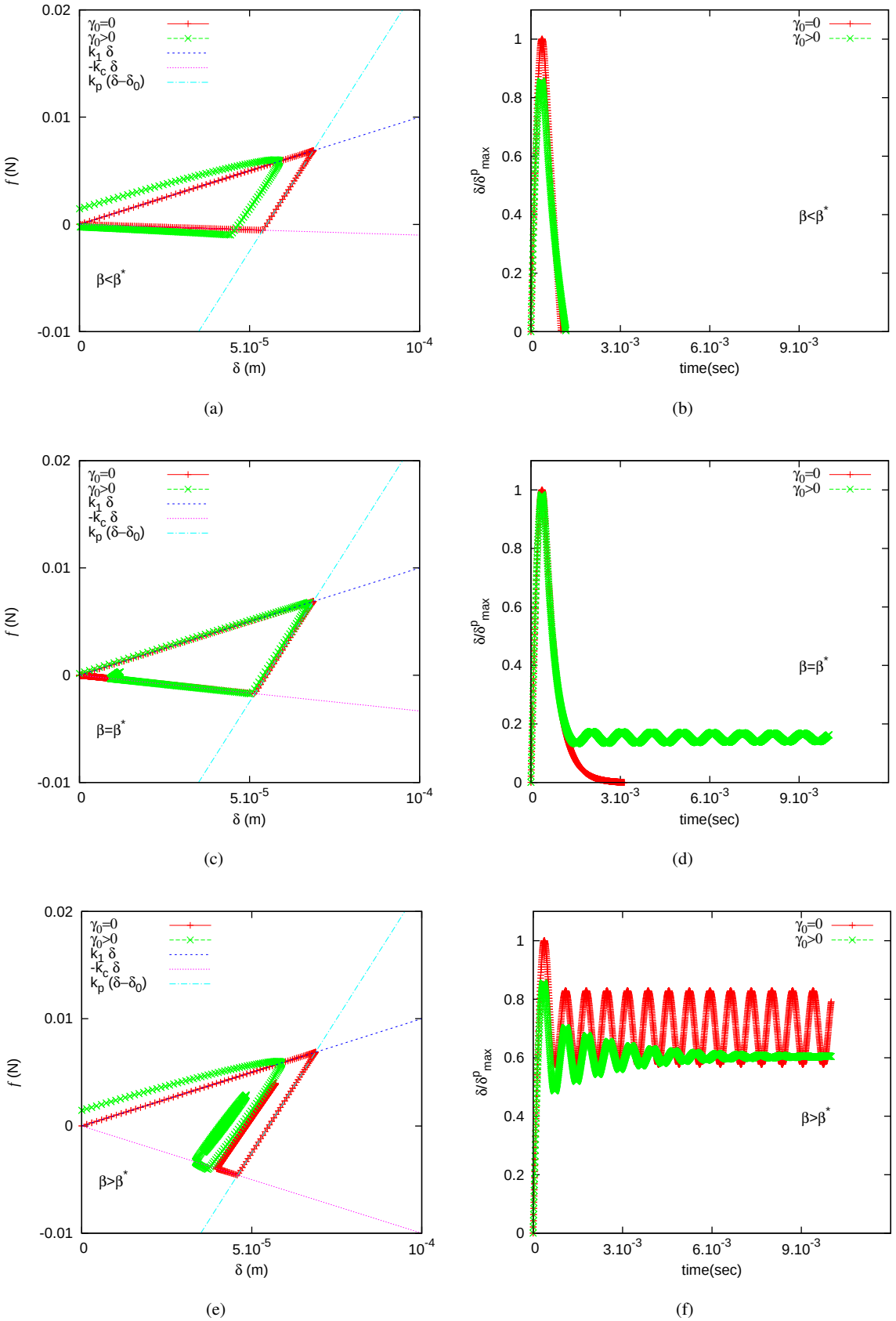

Fig. 11 (a), (c), (e) Contact forces plotted against overlap and (b), (d), (f) time evolution of $\delta/\delta^p_{\max}$ for pair collisions with parameters $k_1 = 10^2$, $k_p = 5 \times 10^2$ and different $k_c = 10$, 33.33, and 100, (units Nm^{-1}), i.e. with $\eta = 4$, $\beta < \beta^*$, $\beta = \beta^*$ and $\beta > \beta^*$, for the same situations as shown in Fig. 10. The red and green symbols represent the data in the presence and absence of viscosity respectively, where $\gamma_0 = 5 \times 10^{-3}$, (unit Nm^{-1}sec).

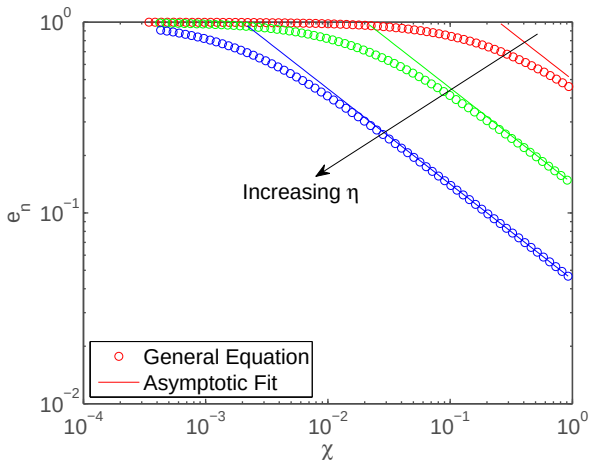

Fig. 12 The coefficient of restitution is plotted against the scaled initial velocity χ in log-log-scale for $\beta = 0$ and three values of $\eta = 5$, 50, and 500, with the other parameters as in Fig. 7. Red, green and blue circles denote, respectively, the solution of Eq. (39), while the solid lines represent the approximation for high scaled impact velocity and large plasticity $\eta \gg 1$.

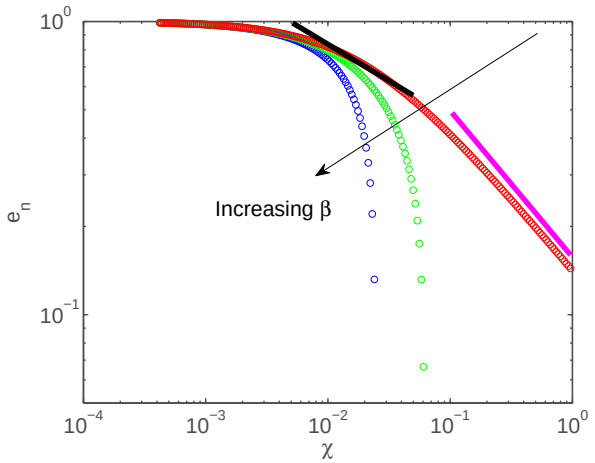

Fig. 13 Log-log plot of the coefficient of restitution against the scaled initial velocity χ for four different values of $\beta = 0.01$, 0.1, and 1.0, with $\eta = 50$. Red, green and blue circles denote the respective solutions of the general equation, Eq. (26), solid black line represents power law $e_n \sim v^{-1/4}$, while magenta line denotes $e_n \sim v^{-1/2}$.

5 Conclusions

In this paper, first, various classes of contact models for (non)linear elastic, adhesive and elasto-plastic particles, are reviewed. The well understood models for perfect spheres of homogeneous elastic or elasto-plastic materials are not considered further. Instead, particular attention is devoted to a elasto-plastic model that can find its main application areas for fine powders and for materials with a plastic external shell and a stiffer core, as described by a limit elastic stiffness k_p. The contact model [18] is extended and generalized by adding short-ranged (non-contact) interactions; the two cases of reversible and irreversible non-contact models are considered. The influence of the model parameters on the overall impact behavior is discussed, focusing on the irreversible, adhesive, elasto-plastic model that is as simple as possible but catches the important phenomena of particle interactions.

When the dependence of the coefficient of restitution, e, on the relative velocity between particles is analyzed, two sticking regimes, $e = 0$, show up, related to different sources of dissipation in the system. (i) The particles stick to each other at very low impact velocity, in agreement with previous results in the literature (see e.g. Refs. [5,28,31]), due to the irreversible short-range interaction. The threshold velocity, below which the particles stick, is directly related to the magnitude of the non-contact adhesive force f_a. (ii) With increasing velocity, e increases and then decreases again until a the second sticking regime is reached, due to the plastic dissipation in the hysteric contact model. While the details of the contact model are of minor importance for small impact velocities, interestingly, for high velocity and small adhesive force f_a, the coefficient of restitution is independent

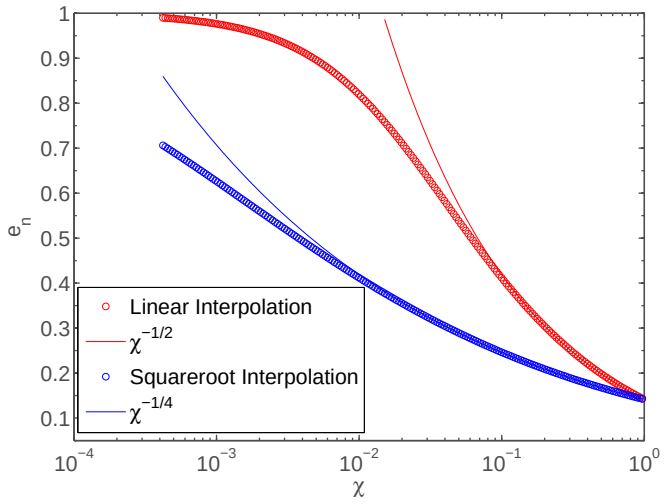

Fig. 14 Semi-log plot of the coefficient of restitution as function of the scaled initial velocity χ, using different interpolation rules for k_2, for pair collisions with $\eta = 50$ and $\beta = 0$. The symbols denote the solutions of the general equation, Eq. (39) with linear interpolation (red circles) or square root interpolation (blue circles), as given in Eq. (41). The red and blue solid lines represent the approximations for high impact velocity $e_n \sim \chi^{-1/2}$ and $e_n \sim \chi^{-1/4}$.

of f_a, i.e., the contribution of the irreversible non-contact force can be neglected in this range.

In the limit of weak f_a, the contact component of the coefficient of restitution is examined analytically, using simple energy conservation arguments. The results are derived in a closed analytical form, by phrasing the behavior in terms of dimensionless parameters (plasticity, adhesivity and initial velocity) and the range of impact velocities for which the second sticking regime is observed, is predicted. For still increasing relative velocity, beyond the sticking region, e_n starts increasing again. However, this regime involves a change of the physical behavior of the system, as e.g. due to fracture/breakage of the particles, and requires additional model assumptions not considered in this paper. Exceptions are fine, inhomogeneous powder particles or core-shell materials, for which the present contact model is suited very well.

The dependence of e_n on the adhesion strength is studied, showing that (high velocity) sticking is observed only if particle adhesion is stronger than a minimum value. In the sticking regime, due to the lack of dissipation on the un-/re-loading branch with stiffness k_2, the sticking particles oscillate around their equilibrium position. A few simulation results with viscosity are also presented, which portray a more realistic physical picture. In the sticking case, for long enough time the particles loose the artificial oscillation energy and stay in static contact with a finite overlap.

In the last part of the paper a section is dedicated to the asymptotic behavior of e_n at high impact velocities. We observe that the law $e_n \sim {v_i}^{-1/2}$, directly related to the empirical choice of the unloading stiffness in the model, is able to describe the variation of e_n for low adhesivity. Further analysis on this feature are postponed to the future, when new data from modern experimental techniques will be available for numerical calibration and validation involving fine powders or core-shell materials.

The application of the present results to many-particle systems (bulk behavior), see Ref. [19] where the non-contact forces were disregarded, is a future goal. An interesting question that remains unanswered concerns a suitable analogy to the coefficient of restitution (as defined for pair collisions) relevant in the case of bulk systems, where particles can be permanently in contact with each other over long periods of time, and where impacts are not the dominant mode of interaction.

6 Acknowledgment

Helpful discussions with N. Kumar and T. Weinhart are appreciated. We thank T. Weinhart for careful and critical reading of the manuscript. Insightful discussions with Prof. Shuiqing Li are also appreciated. We would also like to thank the referees for their constructive criticism and comments that helped us to hugely improve the manuscript.

Financial support (project number: 07CJR06) from a research program of the Stichting voor Fundamenteel Onderzoek der Materie (FOM), which is financially supported by the “Nederlandse Organisatie voor Wetenschappelijk Onderzoek” (NWO), is acknowledged.

Appendix: Energy Picture

This appendix shows the energies of two particles during contact, where the difference between the different branches of the contact model,

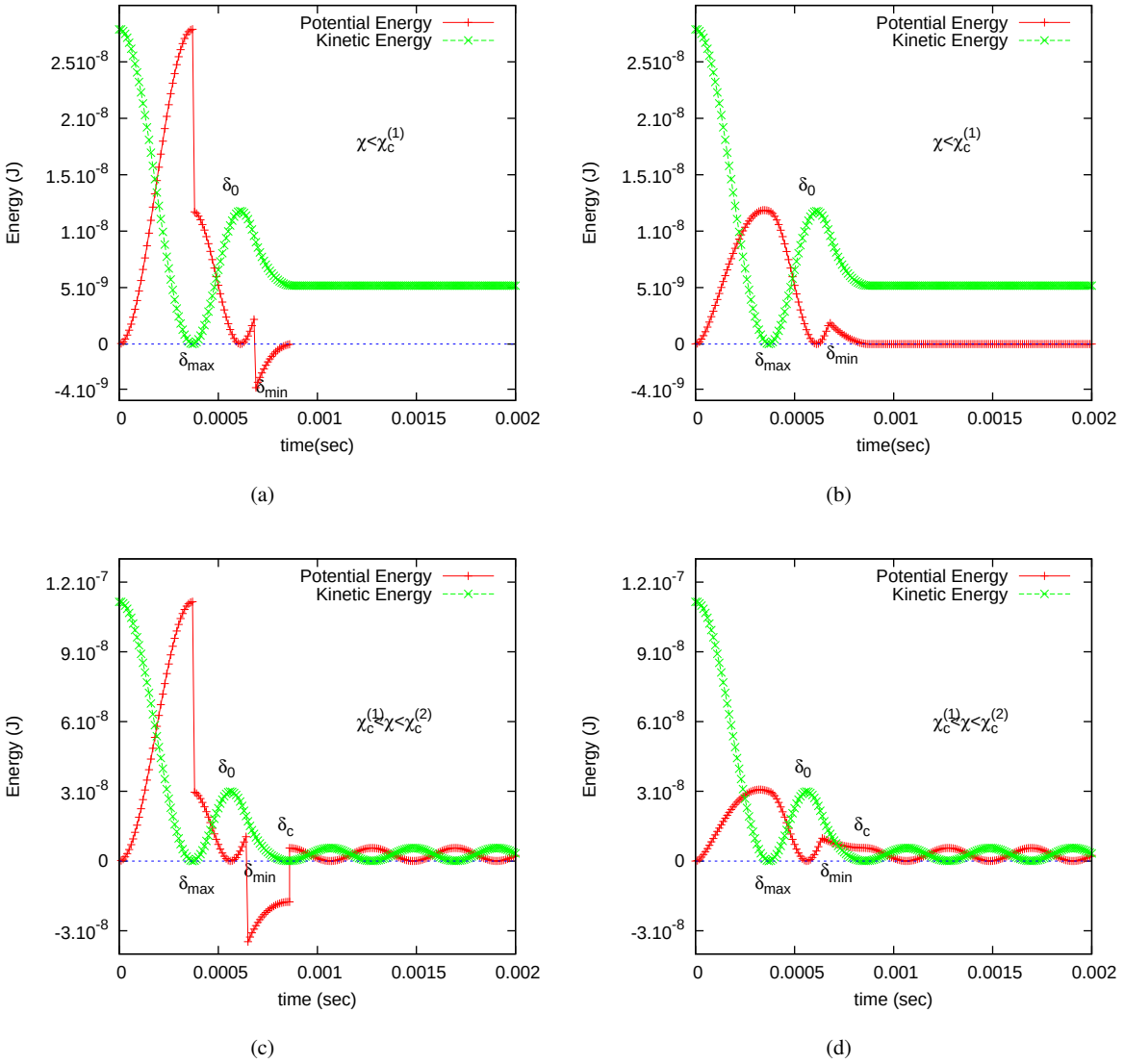

Fig. 15 (a,c) Kinetic and (irreversible, plastic, "potential") energy of the particles, and (b,d) kinetic and available (elastic) potential energy (for re-loading) of the particles, plotted against time for pair collisions with $k_1 = 10^2\,\mathrm{Nm}^{-1}$. $k_p = 5\times10^2\,\mathrm{Nm}^{-1}$, and $k_c = 10^2\,\mathrm{Nm}^{-1}$, i.e. $\eta = 4$ and $\beta = 1$. The initial velocity χ is $\chi = 0.34$ (a,b) and $\chi = 0.69$ (c,d), in the regimes defined in the inset of each plot.

namely irreversible/unstable or reversible/elastic ones, will be highlighted.

In Fig. 15, the time-evolution of kinetic and potential energy is shown; the graphs can be viewed in parallel to Figs. 8(a) and 8(b). In Fig. 15(a), we plot the kinetic and potential energy of the particles against time for low initial velocity $\chi < \chi_c^{(1)}$, corresponding to Fig. 8(a), for which dissipation is so weak that particles do not stick. The kinetic energy decreases from its initial value and is converted to potential energy (the conversion is complete at $\delta_{\max}$). Thereafter, the potential energy drops due to the change between the loading and unloading slope from k_1 to k_2. The potential energy decreases to zero (at the force-free overlap δ_0), where it is converted to (less) kinetic energy. Then the kinetic energy decreases further due to the acting adhesive force. At $\delta_{\min}$ the increasing potential energy drops to a negative value due to the change in unloading slope from k_2 to the adhesive (instable) slope $-k_c$. From there it increases from this minimum, negative value to zero, for $\delta = 0$. From here the kinetic energy remains constant and the potential energy stays at zero, since the particles are separated.

In Fig. 15(b), we plot the time evolution of kinetic and potential energy that the particles would have if un-/re-loading would take place at that moment, along the branch with slope k_2, namely the available (elastic) potential energy. This energy increases from zero at $t = 0$, and reaches a maximum when the kinetic energy becomes zero (note that it is not equal to the initial kinetic energy due to the plastic change of slope of k_2.) Thereafter, the available potential energy decreases to zero at the force-free overlap δ_0. For further unloading, the available potential energy first increases and then drops rapidly on the unstable branch with slope $-k_c$. The change in sign of the unloading slope, from k_2 to $-k_c$, is reflected in the kink in the curve at $\delta_{\min}$. Note, that comparing Figs. 15(a) and 15(b), the available potential energy always stays positive, while the total, plastic "potential" energy drops to negative values after the kink at $\delta_{\min}$.

Figs. 15(c) and 15(d) show the time evolution of kinetic and potential energy (total and available, respectively) for an initial velocity $\chi_c^{(1)} < \chi < \chi_c^{(2)}$ in the sticking regime, see Fig. 8(b). In Fig. 15(c), a similar trend as that of Fig. 15(a) is observed until the potential energy becomes negative at $\delta_{\min}$. The difference to the case of smaller impact velocity is that at this point, the kinetic energy is less than the magnitude of the negative potential energy and hence first reaches zero, i.e., the particles stick. At this point, the (plastic) potential energy increases and jumps to a positive value indicating the change in sign of the unloading slope from $-k_c$ to k_2. Finally, it oscillates between this positive value at δ_c, exchanging energy with the kinetic degree of freedom. When the available potential energy is plotted in Fig. 15(d), a similar trend as that of Fig. 15(b) is observed up to the kink at $\delta_{\min}$. Here, the two energies have comparable values when they reach $\delta_{\min}$ and the kinetic energy decreases to zero with a non-zero available potential energy, which causes the contact to re- and un-load along k_2. /bin/bash: a: command not found

References

1. M. P. Allen and D. J. Tildesley. *Computer Simulation of Liquids*. Oxford University Press, Oxford, 1987.
2. Y. M. Bashir and J. D. Goddard. A novel simulation method for the quasi-static mechanics of granular assemblages. *J. Rheol.*, 35(5):849–885, 1991.
3. N. V. Brilliantov, N. Albers, F. Spahn, and T. Pöschel. Collision dynamics of granular particles with adhesion. *Phys. Rev. E*, 76:051302, Nov 2007.
4. P. A. Cundall and O. D. L. Strack. A discrete numerical model for granular assemblies. *Géotechnique*, 29(1):47–65, 1979.
5. B. Dahneke. Measurements of bouncing of small latex spheres. *Journal of Colloid and Interface Science*, 45(3):584 – 590, 1973.
6. B. Dahneke. Further measurements of the bouncing of small latex spheres. *Journal of Colloid and Interface Science*, 51(1):58 – 65, 1975.
7. B. Derjaguin, V. Muller, and Y. Toporov. Effect of contact deformations on the adhesion of particles. *Journal of Colloid and Interface Science*, 53(2):314 – 326, 1975.
8. A. P. Hatzes, F. Bridges, D. N. C. Lin, and S. Sachtjen. Coagulation of particles in saturn's rings: Measurements of the cohesive force of water frost. *Icarus*, 89(1):113 – 121, 1991.
9. H. J. Herrmann, J.-P. Hovi, and S. Luding, editors. *Physics of dry granular media - NATO ASI Series E 350*, Dordrecht, 1998. Kluwer Academic Publishers.
10. R. Jasevičius, J. Tomas, and R. Kačianauskas. Simulation of normal impact of ultrafine silica particle on substrate. *Particulate Science and Technology*, 29(2):107–126, 2011.
11. K. L. Johnson. *Contact Mechanics*. Cambridge Univ. Press, Cambridge, 1989.
12. K. K. Johnson K. L and R. A. D. Surface energy and the contact of elastic solids. *Proc. R. Soc. Lond. A*, 324(1558):301–313, 1971.
13. G. Kuwabara and K. Kono. Restitution coefficient in a collision between two spheres. *Japanese Journal of Applied Physics*, 26(8):1230–1233, 1987.
14. M. Lätzel, S. Luding, H. J. Herrmann, D. W. Howell, and R. P. Behringer. Comparing simulation and experiment of a 2d granular couette shear device. *Eur. Phys. J. E*, 11(4):325–333, 2003.
15. S. Li, J. S. Marshall, G. Liu, and Q. Yao. Adhesive particulate flow: The discrete-element method and its application in energy and environmental engineering. *Progress in Energy and Combustion Science*, 37(6):633 – 668, 2011.
16. S. Luding. Collisions & contacts between two particles. In H. J. Herrmann, J.-P. Hovi, and S. Luding, editors, *Physics of dry granular media - NATO ASI Series E350*, page 285, Dordrecht, 1998. Kluwer Academic Publishers.
17. S. Luding. Particulate solids modeling with discrete element methods. In P. Massaci, G. Bonifazi, and S. Serranti, editors, *CHoPS-05 CD Proceedings*, pages 1–10, Tel Aviv, 2006. ORTRA.
18. S. Luding. Cohesive, frictional powders: contact models for tension. *Granular Matter*, 10:235–246, 2008.
19. S. Luding and F. Alonso-Marroqun. The critical-state yield stress (termination locus) of adhesive powders from a single numerical experiment. *Granular Matter*, 13:109–119, 2011.
20. S. Luding, E. Clément, A. Blumen, J. Rajchenbach, and J. Duran. Anomalous energy dissipation in molecular dynamics simulations of grains: The "detachment effect". *Phys. Rev. E*, 50:4113, 1994.
21. S. Luding and H. J. Herrmann. Micro-macro transition for cohesive granular media. in: Bericht Nr. II-7, Inst. für Mechanik, Universität Stuttgart, S. Diebels (Ed.), 2001.
22. S. Luding, K. Manetsberger, and J. Muellers. A discrete model for long time sintering. *Journal of the Mechanics and Physics of Solids*, 53(2):455–491, 2005.
23. O. Molerus. Theory of yield of cohesive powders. *Powder Technology*, 12(3):259 – 275, 1975.
24. O. Molerus. Effect of interparticle cohesive forces on the flow behaviour of powders. *Powder Technology*, 20:161–175, 1978.
25. T. Ormel, V. Magnanimo, H. H. ter, and S. Luding. Modeling of asphalt and experiments with a discrete particles method. In *Conference Proceedings MAIREPAV7 2012*, 2012.
26. D. C. Rapaport. *The Art of Molecular Dynamics Simulation*. Cambridge University Press, Cambridge, 1995.
27. K. Saitoh, A. Bodrova, H. Hayakawa, and N. V. Brilliantov. Negative normal restitution coefficient found in simulation of nanocluster collisions. *Phys. Rev. Lett.*, 105:238001, Nov 2010.
28. C. Sorace, M. Louge, M. Crozier, and V. Law. High apparent adhesion energy in the breakdown of normal restitution for binary impacts of small spheres at low speed. *Mechanics Research Communications*, 36(3):364 – 368, 2009.
29. C. Thornton. Numerical simulations of deviatoric shear deformation of granular media. *Géotechnique*, 50(1):43–53, 2000.
30. C. Thornton, S. J. Cummins, and P. W. Cleary. An investigation of the comparative behaviour of alternative contact force models during elastic collisions. *Powder Technology*, 210(3):189 – 197, 2011.
31. C. Thornton and Z. Ning. A theoretical model for the stick/bounce behaviour of adhesive, elastic-plastic spheres. *Powder Technology*, 99(2):154 – 162, 1998.
32. C. Thornton and K. K. Yin. Impact of elastic spheres with and without adhesion. *Powder Technol.*, 65:153, 1991.
33. C. Thornton and L. Zhang. A dem comparison of different shear testing devices. In Y. Kishino, editor, *Powders & Grains 2001*, pages 183–190, Rotterdam, 2001. Balkema.
34. J. Tomas. Particle adhesion fundamentals and bulk powder consolidation. *KONA*, 18:157–169, 2000.
35. J. Tomas. Assessment of mechanical properties of cohesive particulate solids. part 1: Particle contact constitutive model. *Particulate Science and Technology: An International Journal*, 19:95–110, 2001.
36. J. Tomas. Assessment of mechanical properties of cohesive particulate solids. part 2: Powder flow criteria. *Particulate Science and Technology: An International Journal*, 19:111–129, 2001.
37. P. A. Vermeer, S. Diebels, W. Ehlers, H. J. Herrmann, S. Luding, and E. Ramm, editors. *Continuous and Discontinuous Modelling of Cohesive Frictional Materials*, Berlin, 2001. Springer. Lecture Notes in Physics 568.
38. L. Vu-Quoc and X. Zhang. An elastic contact force-displacement model in the normal direction: displacement-driven version. *Proc. R. Soc. Lond. A*, 455:4013–4044, 1999.
39. H.-C. W. Wall S., Walter J. and G. L. S. Some experiments on anelastic rebound. *Aerosol Science and Technology*, 12(4):926 – 946, 1990.

40. O. R. Walton and R. L. Braun. Viscosity, granular-temperature, and stress calculations for shearing assemblies of inelastic, frictional disks. *J. Rheol.*, 30(5):949–980, 1986.
41. X. Zhang and L. Vu-Quoc. Simulation of chute flow of soybeans using an improved tangential force-displacement model. *Mechanics of Materials*, 32:115–129, 2000.